Int. J. Heat Mass Transfer. Vol. 33, No. 12, pp. 2585–2598, 1990
Printed in Great Britain

0017-9310/90 $3.00 + 0.00

Hydrodynamic, thermal and crystallographical effects of an electromagnetically driven rotating flow in solidifying aluminium alloy melts

CHARLES VIVES

Université d'Avignon, Laboratoire de Magnétohydrodynamique, 33, rue Louis Pasteur, 84000 Avignon, France

(*Received* 5 *October* 1989)

Abstract—The influence of rotating aluminium alloy flows, driven by a stationary electromagnetic field, during freezing in a toroidal mould, is studied. The experiments are performed in the absence, and in the presence, of forced cooling. The important role of the centrifugal acceleration on the evolution during freezing of the velocity, temperature, and solid fraction distributions in the two-phase mixture is revealed. For the case of an alloy characterized by a wide crystallization range, the rotation of the solidifying melt results in a decided refinement of the equiaxed structure. Furthermore, an experimental technique allowing the determination of the electrical conductivity of the melt above the liquidus temperature, as well as inside the freezing range, is proposed.

1. INTRODUCTION

OVER THE last two decades, owing to their impact on industrial casting processes, an increasing interest has been shown in fundamental and applied investigations bearing on metal solidifications, either in the presence of free convection [1–6], or when various dynamic treatments, generating forced convection, are applied in the melt during freezing [7–14]. In relatively recent papers [15–17] comparative studies describing the thermal and crystallographical effects of natural, damped and forced convections during the controlled solidification of a pure metal (tin) have been presented. These experiments, mainly characterized by a directional dendritic growth, have revealed the spectacular impact of the flow structure during solidification and showed that the application of magnetic fields of adequate pattern and strength may be an efficient method for the production either of large single crystals, or of columnar crystals of required shape and size, without pollution of the metal.

However, in industrial production of ferrous and non-ferrous alloys, which is obviously of great commercial importance, equiaxed dendritic or non-dendritic solidification is much more desirable, from many standpoints, than columnar solidification. Indeed, fine-grained structures have improved low temperature strength and toughness, reduced anisotropy, reduced micro-segregation, better heat treatment and reduced hot tearing tendency. Furthermore, grain refining offers substantial improvements in both conventional and continuous casting processes by increasing the casting speed, reducing cracking and cold shots and improving the surface quality of the ingots.

The addition of a nucleating agent is a commonly adopted method in d.c. casting of aluminium alloys [10] and it is well known that inoculation of small amounts of grain refiners master alloys, as Al–5% Ti–1% B (AT_5B), results in a significant reduction of the crystal size. However, the addition of grain refiners may cause negative secondary effects reducing the quality of the metal. For instance, this technique can be detrimental to the quality of the finished product, due to the presence of conglomerates of TiB_2 in the metal. Moreover, the refinement may become practically ineffectual, when the efficiency of the filtering system is sufficiently high to retain a large part of the nuclei of TiB_2 before casting. Furthermore, high strength aluminium alloys, especially those containing zirconium and lithium, are historically difficult to grain refine with conventional titanium–boron–aluminium master alloys [18, 19].

A number of examples can be found in the literature where external forces have been applied to induce fluid flow during solidification in order to refine the grain size. The methods include application of sonic or ultrasonic vibrations, rotation of the mould, mechanical or electromagnetic stirring of the melt [8–15]. Under these conditions, grain structures of castings and ingots change, from columnar-dendritic to equiaxed-dendritic, when they are solidified in the presence of a sufficiently intense liquid convection, which generally promotes the evacuation of superheat. This effect is mainly attributed to grain multiplication: the suspended nuclei localized in the near vicinity of the solid interface, i.e. in the mushy zone, are carried away and dispersed in a slightly undercooled melt. Under these circumstances, the crystallization takes place simultaneously in most of the sump, around a number of floating nuclei, and this increasing nucleation results in the appearance of a fine grained equiaxed structure.

NOMENCLATURE

$\mathbf{B}_0$	externally imposed magnetic field
$\mathbf{b}_0$	magnetic field induced by $\mathbf{J}_0$
$\mathbf{b}$	magnetic field induced by $\mathbf{j}$
$\mathbf{B}$	resultant magnetic field
D	average diameter of the equiaxed crystals
$\mathbf{E}$	electric field
f_s	solid fraction
g	gravity
H	liquid metal height
I_0	externally imposed direct current
$\mathbf{J}_0$	externally imposed current density
$\mathbf{j}$	current density induced by the melt motion
$\mathbf{J}$	resultant current density
M	Hartmann number, $\mathbf{B}_0 H(\sigma/\eta)^{1/2}$
Q	flow rate
r	radial position
Re'	Reynolds number, $U_m H\rho/\eta$
R_e	outer radius of the crucible
R_i	inner radius of the crucible
R_m	magnetic Reynolds number, $\sigma\mu U_m H$
T_0	initial temperature of the bulk liquid
T_l	liquidus temperature
ΔT	superheat, $T_0 - T_l$
U	local velocity
U_m	average velocity
V	voltage
z	vertical position (from the mould bottom).

Greek symbols

η	viscosity of the liquid metal
η_a	apparent viscosity of the liquid–solid mixture
ν	kinematic viscosity
ρ	density
σ	electric conductivity of liquid.

Such mechanisms involve necessarily the appearance of two-phase flows in the melt during stirring, which result in a variation of the apparent viscosity as a function of the solid fraction. Recently, the role of fluid flow and turbulence on the flotation or sedimentation of the solid particles, for given solid fraction and particle size, has been examined by Ilegbusi and Szekely [20]. This investigation was led for the case of gently agitated melts, characterized by a newtonian behaviour.

The aim of this work is to study the hydrodynamic, thermal and crystallographical effects, which appear during solidification of aluminium alloys, in the presence of crossed electric and magnetic fields. In order to compare the findings obtained from aluminium alloys with those corresponding to pure metals, the experiments were once again performed using the same mould and under very near electromagnetic and thermal conditions than those described in recent papers [15–17].

Such an arrangement, where the electromagnetic forces cause the molten metal to rotate rather rapidly, constitute a representative case of easy to control stirring, which is especially encountered in steelmaking practice, where the rotating flows are generated by another electromagnetic technique using rotary induction motors [13]. Tubular castings produced in permanent moulds by centrifugal castings usually have higher yields and higher mechanical properties than castings produced by the static casting process. Finally, a new emerging process consisting in centrifugal casting of composite melts containing particle dispersions should be cited. In particular, centrifugal casting of aluminium–zircon and aluminium–graphite composites produces either a hard abrasion-resistant surface, or wear-resistant solid-lubricated surfaces for such antifriction applications as bearings or cylinder liners [21].

2. EXPERIMENTAL APPARATUS AND PROCEDURE

Only the main features of the device will be described here as the experimental system has already been described in detail elsewhere [15].

The apparatus consisted of a toroidal crucible, made of stainless steel, containing about 2 dm^3 of aluminium alloys with a free surface. The outer cylinder of 174 mm i.d. was resistance heated, while the inner cylinder of 24, or 42 mm o.d. (depending on the experiments), was internally cooled by water at 20°C, with a flow rate of 1000 dm h^{-1}. All the exterior walls of the furnace were thermally insulated.

A stationary magnetic field $\mathbf{B}_0$, parallel to the gravitational force field vector, uniform to 2% inside the melt, was generated by an inductor made up of 248 jointed turns traversed by a direct current, liable to vary within the range of 0–165 A, whereas the corresponding strength B_0 was included between 0 and 0.1 T. Furthermore, a constant voltage was applied between the inner and outer cylinders of the crucible; these walls, playing the role of electrodes, permitted the flow of a radial direct current I_0 (between 0 and 425 A) through the solidifying metal to take place.

The working material used in this investigation was a 2024 aluminium alloy (Al, 92.2%; Cu, 4.2%; Mg, 1.6%; Si, 0.5%; Fe, 0.5%; Mn, 0.7%; Ti, 0.15%; other impurities, 0.15%; liquidus: 645°C; solidus: 485°C), which is an aeronautic alloy, characterized by a wide freezing range, i.e. a large difference between

the liquidus and solidus temperatures. However, some macrographies of 1050 aluminium alloy (Al, 99.5% and traces of Si, Fe, Cu, Mn, Mg, Zn and Ti; liquidus: 664°C; solidus: 635°C) will be displayed. Indeed, this alloy represents a typical case, corresponding to a narrow freezing range, which is due to the small amount of alloying elements contained within this material.

Six thermocouples were placed horizontally at prescribed heights within the melt (Fig. 1), their outputs being fed to a six-channel recorder, so as to follow both the evolution of the solidification front and of the temperature distribution inside the bulk liquid with time. Each experiment was performed by melting the aluminium alloy and heating it to 10°C above the required superheat temperature, at this moment the heating was cut off so that the liquid could cool slowly to the required superheat temperature T_0. Then, the ingots were solidified by delivering cooling water from an initial superheat of ΔT°C above the liquidus temperature T_l. This procedure generates a typical case of radial and outward solidification starting from the inner cooling pipe.

Furthermore, about 1 min before cooling, the tin-pool was simultaneously subjected both to an externally imposed axial and stationary magnetic field and to a radial electric field, giving rise to a tangential electromagnetic body force distribution, throughout the melt (Fig. 1). Hence, the system behaved as an annular electromagnetic conduction pump and the liquid was set in rotation under the action of the steady electromagnetic force pattern.

However, another set of freezing experiments has been carried out in the absence of water cooling, in order that solidification takes place slowly and without a preferential growing direction.

Subsequently, each ingot was sectioned, polished and etched to reveal its grain structure.

3. DIRECTIONAL SOLIDIFICATION IN THE PRESENCE OF FORCED COOLING

3.1. *Velocity measurements*

One of the attractions of this system is that a steady electromagnetic field could be used, thereby bypassing the difficulty of weak field penetration deep into the solidifying melt when alternating fields are used to promote mixing during metallurgical processes (electromagnetic skin effect). Moreover, on account of the very weak value of the electric resistance of the bath (of the order of 10^{-5} ohm), and contrary to the case of stirring generated by travelling magnetic fields, the electric power consumption is practically insignificant. Lastly, the strength of the electromagnetic body forces and, hence, the stirring intensity, may be easily modulated at will by variation of the magnitudes of $\mathbf{B}_0$, or I_0.

The velocity measurements were carried out using an incorporated magnet probe [22, 23]. The readings yielded by the nanovoltmeter connected with the velocity probe were recorded and the end of the fluid flow acceleration period was revealed by a nearly constant measurement, reached after a transient time of about 30 s. In order to eliminate the parasitic voltage due to the presence of an electric field $\mathbf{E}$ in the melt, the magnetic field $\mathbf{B}_0$ and the electric current I_0 could then be simultaneously interrupted to get the azimuthal velocity at a selected location.

Figure 2(a), corresponding to the starting point of solidification, i.e. $R_i = 1.2$ cm, shows tangential velocity profiles plotted along a radius, at mid-height of the melt, with a constant magnetic field and for different values of the electric current I_0. The Hartmann number M, which is proportional to the magnetic field B_0, has already been defined [16]. It appears in Fig. 3 that, for a given value of M, the flow rate Q through a radial and vertical cross-section tends

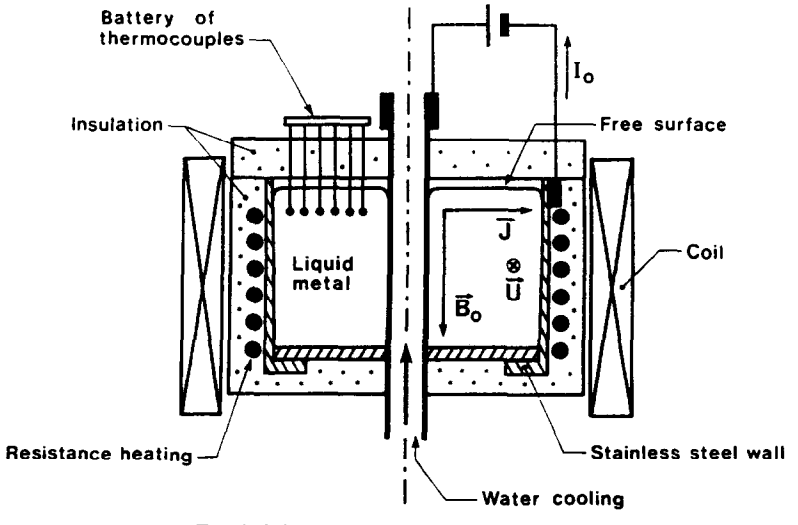

FIG. 1. Schematic diagram of the apparatus.

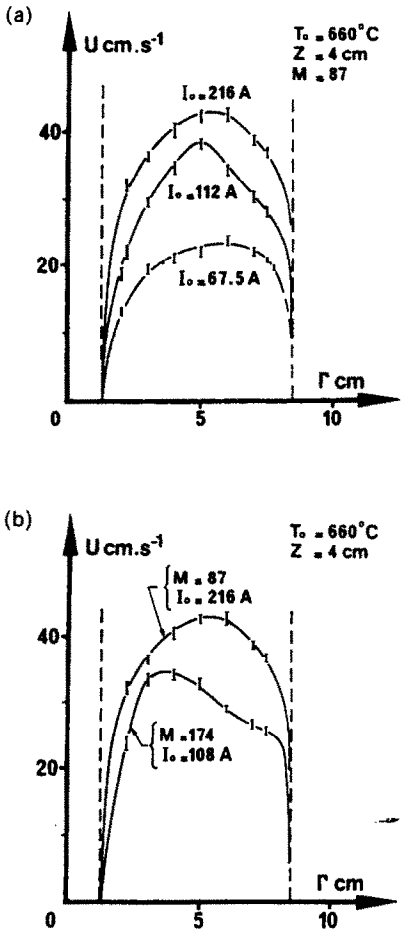

FIG. 2. Tangential velocity profiles as a function of the radial position plotted at mid-height of the melt: (a) for different values of the B_0I_0 product (or MI_0); (b) for the same value of the B_0I_0 product (or MI_0).

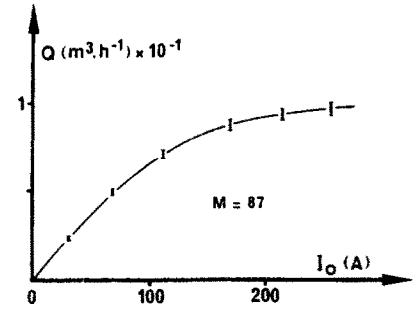

FIG. 3. Variation of the flow rate Q, determined at the onset of freezing, as a function of the imposed electric current I_0, for a given value of the magnetic field B_0 (or of the Hartmann number).

asymptotically to a limit, when the imposed current intensity I_0 increases.

Figure 2(b) depicts distributions of the tangential velocity, plotted for a constant value of B_0I_0 (or MI_0); the flow rate increases with the current I_0. In fact,

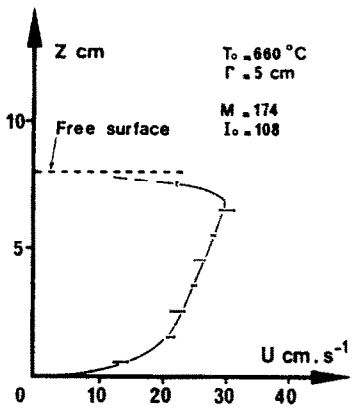

FIG. 4. Tangential velocity profile as a function of the vertical position, plotted for $r = 5$ cm.

when the liquid metal is set in rotation, an induced current of density j (caused by an induced e.m.f. due to the Lorentz law) arises. Hence, particularly within the hydrodynamic boundary layers [24], additional body forces appear which are opposite to the externally imposed forces, and which are all the more weakened as B_0 is stronger. So, it will be interesting, to obtain high velocities, to operate with intense current and low magnetic field, more especially as strong magnetic fields are not easily generated in large volume.

Figure 4 shows that, for a given radial position, the tangential velocity varies linearly with the vertical position, except in the vicinity of the mould bottom (no slip conditions) and of the liquid free surface. Moreover, at the onset of freezing a unicellular fluid motion (with velocity peaks of the order of 4 cm s^{-1}), mainly located in the upper half of the pool, has been detected inside a radial cross-section. Figure 5 presents the evolution of the mean velocity U_m with the position of the solidification front of average diameter R_i and reveals the decay of the electromagnetically driven fluid flow inside the aluminium pool during freezing. This damping is caused both by the increasing surface area of the melt–solid interface, which results in an enhancement of the viscous frictional forces, and by the decline of the electromagnetic

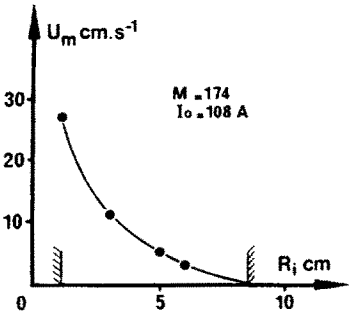

FIG. 5. Variation of the mean velocity in the aluminium melt as a function of the averaged position of the solidifying crust.

body forces $\mathbf{J}\times\mathbf{B}$ acting on a unit volume of the fluid. Indeed, $\mathbf{J}\times\mathbf{B}$ is nonuniform; the forces decrease along a radius, from the inner cylinder to the outer one, on account of Kirchhoff's first law: div $\mathbf{J}=0$.

Although the magnetohydrodynamic aspect of this problem will be not thoroughly examined here, it is necessary to note that the externally imposed electromagnetic field $\mathbf{J}_0\times\mathbf{B}_0$ is modified inside the moving molten metal and must be replaced by the product $\mathbf{J}\times\mathbf{B}$, with $\mathbf{J}=\mathbf{J}_0+\mathbf{j}$, where $\mathbf{j}$ is the electric current density induced by the interaction of the fluid velocity $\mathbf{U}$ with the magnetic field $\mathbf{B}$, and $\mathbf{B}=\mathbf{B}_0+\mathbf{b}_0+\mathbf{b}$, where $\mathbf{b}_0$ is the magnetic field generated by the externally applied current density $\mathbf{J}_0$ ($\mu_0\mathbf{J}_0=\mathbf{Curl}\,\mathbf{b}_0$) and $\mathbf{b}$ the magnetic field generated by the induced current $\mathbf{j}$ ($\mu_0\mathbf{j}=\mathrm{Curl}\,\mathbf{b}$). The ratio of the induced magnetic field $\mathbf{b}$ to the externally imposed magnetic field $\mathbf{B}_0$ is of the order of $\sigma\mu UH$, which is the magnetic Reynolds number R_m [24]. Under our experimental conditions, the maximum value $b/B_0\simeq 0.1$, is obviously reached in the early stages of solidification.

3.2. *Temperature measurements*

3.2.1. *Natural convection.* The isotherm maps presented in Fig. 6 have been obtained with a 2024 aluminium alloy and from an initial superheat of 25°C. Figure 6(a) displays a temperature field plotted at the initiation of freezing ($t=15$ s). It is seen that the isotherms are nearly parallel to the melt–solid interface in its vicinity, while the vertical and radial isothermal gradients are relatively weak. Moreover, the shape of both the solidification front and the isotherms indicates, at least in the initiation of outward freezing, the very probable presence of a convective cell located in the right upper part, which corresponds to the hotter zone of the melt. Figure 6(b), plotted for $t=30$ s, shows that the shape of the isotherms is not considerably affected, on the other hand the average superheat drop is 29°C.

3.2.2. *Electromagnetic stirring.* Examination of Figs. 6(c) and (d) yields support to the presence of a main recirculating vortex, located in the upper region and already detected from velocity measurements. The two hotter zones are respectively situated in the vicinity of the lower-right-hand-side corner and of the free surface. Moreover, the interface shape is influenced by the secondary flows which are likely to appear under the condition of rotating flows [17, 25, 26].

Figure 7 shows, once again, that the dissipation of

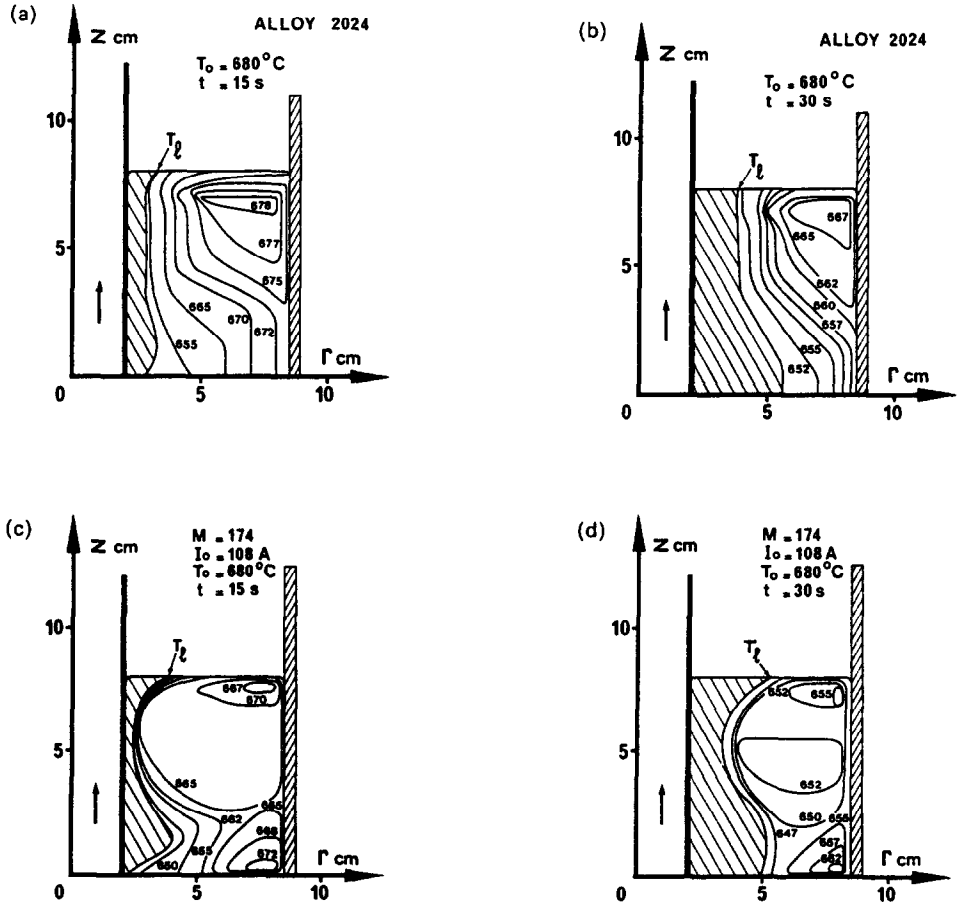

FIG. 6. Evolution of isotherm maps with time, in natural convection: (a) $t=15$ s, (b) $t=30$ s, and in the presence of crossed electric and magnetic fields (c) $t=15$ s, (d) $t=30$ s.

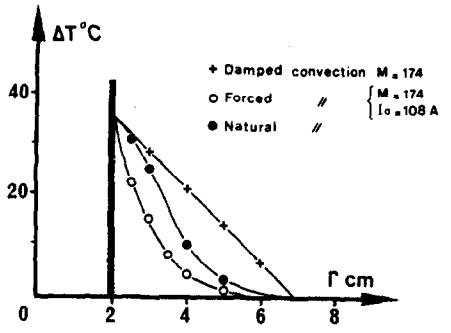

FIG. 7. Superheat drop as a function of the thickness of the solidifying crust in natural, forced and damped convection.

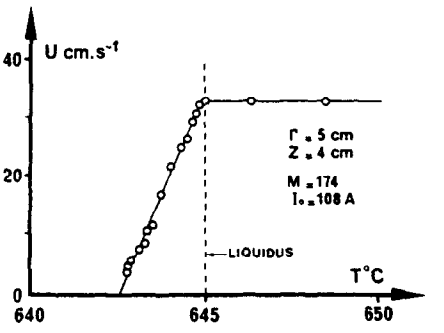

FIG. 8. Example of evolution of the local tangential velocity as a function of the temperature, in the presence of electromagnetic stirring.

superheat is accelerated by forced convection. The velocity being mainly tangential does not contribute directly to an efficient mixing between the hot and cold wall regions, but the turbulence intensity is probably high enough to promote a rapid transfer to the fluid layers, at least in the early stages of freezing, where the Reynolds number $Re = U_m H/\nu$ can reach 40 000. Moreover, notwithstanding the weakness of the velocities inside the main recirculating vortex (of the order of 5 cm s^{-1}), the impact of this flow must be considered, because under this circumstance, the fluid particles carried away by the secondary loop travel alternately from a hot to a cold zone. Hence, this secondary flow contributes certainly to the uniformity of the temperature in the central bulk (Fig. 6).

When the electric current I_0 is cut off, the liquid metal is only subjected to the magnetic field B_0. This situation results in a pronounced damping of the fluid flow [16] and it is seen in Fig. 7 that, in contrast with the case of forced stirring, the escape of superheat is markedly delayed by the application of a stationary magnetic field.

4. SOLIDIFICATION IN THE ABSENCE OF FORCED COOLING

In these experiments, the solidification takes place slowly, without a preferential growing direction, inside a non-water cooled metal mould. Such a procedure corresponds to a widespread industrial production of static ingots cast in a mould (a sand mould, for example).

The basic experimental technique used was to measure simultaneously the temperature and the velocity as a function of time, at a series of points, within the solidifying 2024 alloy. To this end, a thermocouple was fastened to the velocity probe.

4.1. *Velocity measurements*

Figure 8 shows that the tangential velocitiy U, generated by electromagnetic stirring, varies linearly with the temperature drop from the liquidus and that the alloy is practically stagnant, when the temperature is about 2.5°C below the liquidus.

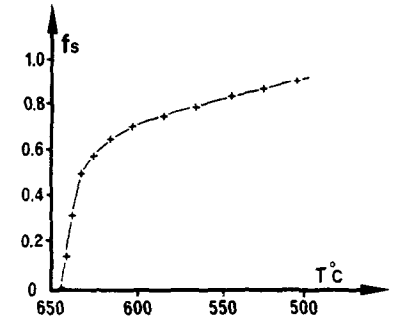

FIG. 9. Variation of the solid fraction in a 2024 aluminium alloy melt as a function of the temperature.

Figure 9 displays the evolution of the solid fraction f_s as a function of the temperature; it appears that, at the initiation of freezing, f_s is directly proportional to the temperature drop (the slope being 4.5% f_s per °C). It follows that, under these experimental conditions, the velocity U and the apparent viscosity η_a depend linearly on the solid fraction. Moreover, systematical experiments, consisting in alternate freezing and melting inside the range 645–642.5°C, showed that the velocity measurements were reversible and time independent. So, one may legitimately assume that, for the stirring intensities imposed in this investigation, the liquid–solid mixture is characterized by a Newtonian behaviour. On the other hand, the two-phase medium localized within the mushy zone behaves, from the consistency standpoint, practically as a solid when the temperature of the bath is 3°C below the liquidus temperature, dealing with an amount of about 13% of suspended particles into the melt.

Figure 10 conveys azimuthal velocity profiles, plotted at a given time, along a radius. The starting time ($t = 0$) corresponds to the liquidus temperature. Experiments carried out above the liquidus showed that, under this circumstance where the mould is not water cooled, the melt is practically isothermal throughout the crucible. On the contrary, it is seen that below the liquidus, thermal gradients appear (in Fig. 10, each number placed above a star denotes the

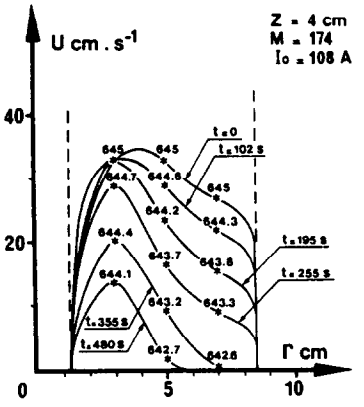

FIG. 10. Tangential velocity profiles plotted at different times during freezing.

temperature at a given time and for a given radial position). It is seen that the flow rate decreases gradually with time. After 350 s, the liquid metal flows only inside a peripheral area surrounding the inner cylinder, whereas the alloy is stagnant within a zone located in the vicinity of the outer wall; this latter region grows larger and larger during solidification.

At first glance, this finding may seem paradoxical because, on account of the thermal inertia of the insulating material placed round the resistance heating (Fig. 1), the external face of the outer wall is hotter than the inner pipe, which is not water cooled and only in contact with air. This accumulation of solid particles is caused by the centrifuging action of the rotation on the suspended crystals, already growing in the liquid phase. The particles, subjected to centrifugal forces, being denser than the liquid move radially outwards. Actually, under our experimental conditions, where the maximum value of the tangential velocity U reaches 0.6 m s^{-1}, the centrifugal acceleration U^2/r may be of the order of $5g$, at the onset of freezing.

4.2. *Temperature measurements*

Temperature distributions, plotted at a given time, are displayed in Fig. 11. Owing to the liquid–solid separation, provoked by the centrifugal forces applied to the growing crystals, and in contrast with the directional solidification in the presence of water cooling (Fig. 6), the melt temperature is not homogenized. The rotating stirring results in the appearance of radial temperature gradients, which increase with time (Fig. 11(b)). Contrary to the case of conventional solidification, where the mushy zone is nearly isothermal (Fig. 11(a)), the colder zone, constituted by the accumulation of solid particles, is located in the neighbourhood of the outer cylinder (Fig. 11(b)). This event is corroborated by inspection of Fig. 12, which illustrates the evolution of the solid fraction profiles with time, in the absence and presence of electromagnetic rotation.

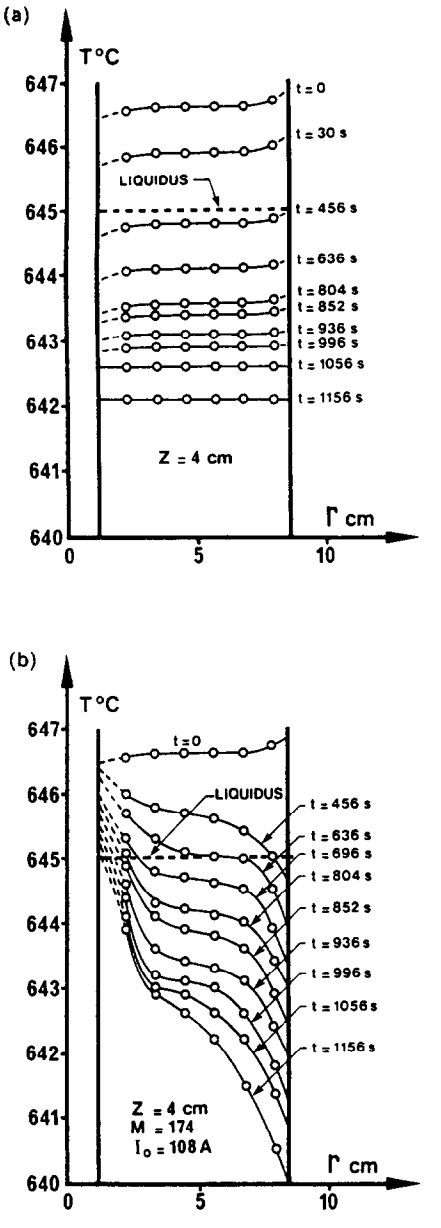

FIG. 11. Evolution of temperature profiles plotted along a radius, for a given vertical position, during freezing: (a) conventional solidification; (b) rotating stirring.

5. REMARKS ON THE ELECTRICAL CONDUCTIVITY OF THE LIQUID–SOLID MIXTURE

In the absence of a magnetic field, the electrical conductivity σ of a liquid metal traversed by a d.c. current I_0, can be determined using a calibrated potential sensor [27, 28]. This probe collects between its two electrode tips AA′, which are separated by a distance l, the e.m.f. V caused by the circulation of the electric field E along a current line (Fig. 13).

The distance l being small, of the order of 2 mm,

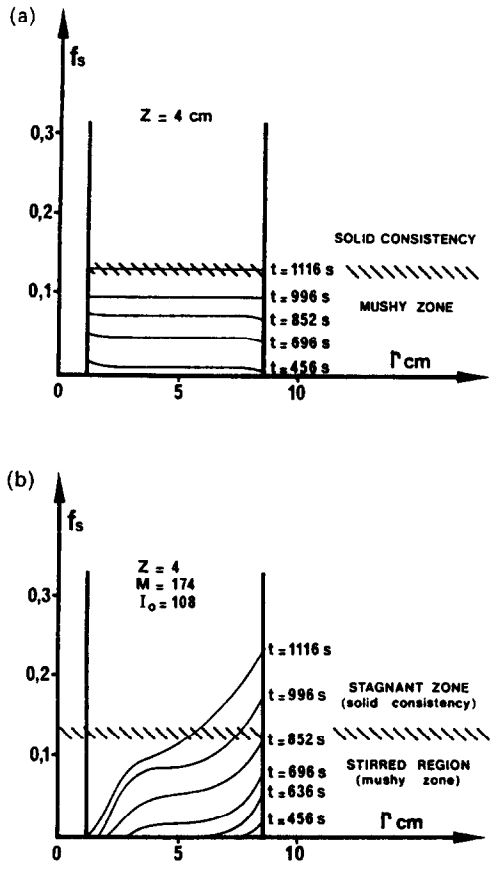

FIG. 12. Evolution of the solid fraction profiles with time: (a) in the absence; and (b) in the presence of electromagnetic rotation.

the measured voltage is given by

$$V = \int_{A}^{A'} \mathbf{E} \cdot d\mathbf{l} = E \cdot l$$

and the current density by

$$J_0 = \sigma E = \sigma V / l$$

J_0 being locally determined by the passage of the imposed d.c. current I_0, flowing radially through the solidifying metal (Fig. 1), it follows that the σV product is constant, whatever the local temperature in the melt.

Consequently, the electrical conductivity measurements were performed according to the following procedure (which is schematically presented in Fig. 13):

(i) the magnetic field B_0 being suppressed, the potential sensor was placed at a given point of the metal pool, while the electrode tips were positioned along a radius (i.e. along an electric current line);

(ii) a thermocouple was fastened to the probe, thus allowing the simultaneous recordings of the temperature T and of the voltage $V(T)$;

(iii) the mould being water cooled, according to the experimental conditions described in Sections 2 and 3 (directional solidification), the two sensors were caught during the advancement of the solidifying crust.

Figure 14 presents the variation of the electrical conductivity, given by $\sigma(T) = \sigma_l V_l / V(T)$ as a function of the temperature (σ_l is the electrical conductivity, at the liquidus temperature T_l, and V_l the corresponding voltage measurement). It should be emphasized that such a technique can be applied whatever the alloy, after comparison with a reference material, the electrical conductivity of which is known. This method, which is relatively easy to put into practice, may prove interesting because the electrical properties of a large majority of aluminium alloys could not be found in the literature.

Finally, the empirical relationship between σ and

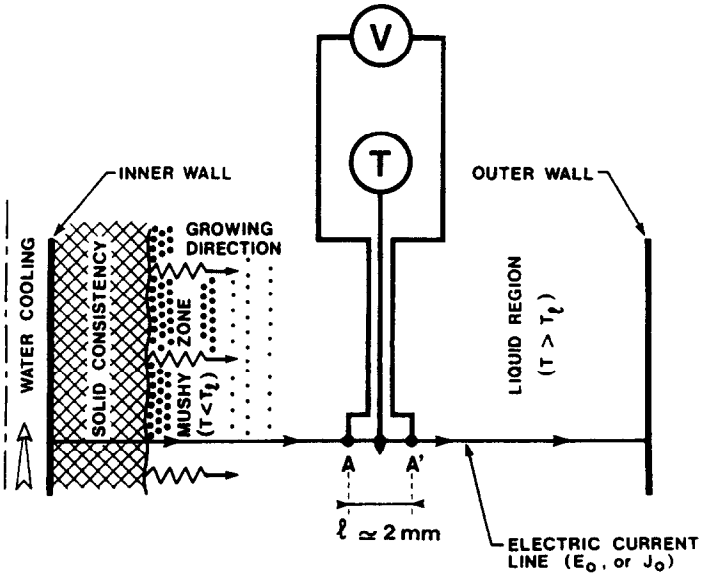

FIG. 13. Principle of electric current density measurements during freezing.

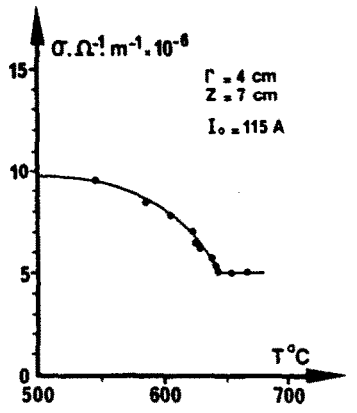

FIG. 14. Variation of the electrical conductivity of the 2024 aluminium alloy as a function of the temperature.

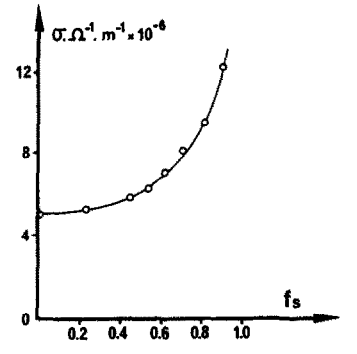

FIG. 15. Variation of the electrical conductivity of the 2024 aluminium alloy as a function of the solid fraction.

the solid fraction is readily reached (Fig. 15). It occurs that within the range $0 < f_s < 13\%$, where the liquid–solid mixture is likely to flow, σ increases very slowly. As a result, the current density which is connected with the electrical conductivity, through Ohm's law for moving media, $\mathbf{J} = \sigma(\mathbf{E} + \mathbf{U} \times \mathbf{B})$ and, in turn, the electromagnetic force field $\mathbf{J} \times \mathbf{B}$, responsible for the stirring intensity, are not markedly altered in the course of solidification. Accordingly, the decay of the fluid flow during freezing can be primarily attributed to the increasing apparent viscosity of the medium.

6. CRYSTAL GROWTH

The macrostructures of a 2024 aluminium alloy, displayed in Figs. 16 and 18, have been respectively obtained in the presence and absence of water cooling. The primary effect that has been observed, when the melt is subjected to electromagnetic stirring, is that rotation of the liquid as it is solidifying causes grain refinement.

In the presence of water cooling (Fig. 16(b)), nucleation is enhanced by viscous shear in the solidifying alloy. This may be understood by the removal of dendrite tips from the solidification front (Figs.

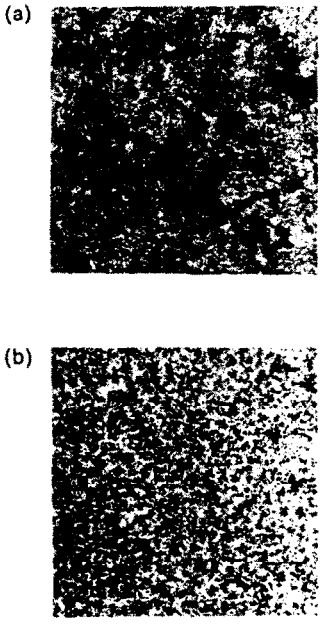

FIG. 16. Macrostructures of a 2024 aluminium alloy, solidified in natural convection, (a) $\Delta T = 35$ C, and in the presence of crossed electric and magnetic fields, (b) $\Delta T = 35$ C, $M_0 = 87$, $I_0 = 250$ A, flow rate of cooling water: 1000 dm^3 h^{-1}; size of the samples: 35 × 35 mm.

6(c) and (d)) by the viscous forces that are set up (Fig. 2(a)). The multiplication of these dendrite fragments results in an increasing number of floating nuclei in the melt [28]. Figure 17 shows the impact of the externally imposed electric current I_0 on the mean equiaxed grain diameter D (for a given value of the magnetic field B_0). It can be seen that D decreases, first rapidly and then asymptotically, when I_0 increases. This effect is partially explained by the fact that the maximum velocity and, in turn, the shear stress tend to a limit, when I_0 increases (Figs. 2(a) and 3). For $I_0 = 425$ A and $B_0 = 5 \cdot 10^{-2}$ T, the average grain size is about 200 μm and the number of equiaxed grains is multiplied by about 15 000, with respect to the case of conventional solidification (Fig. 16(a)).

Figure 18(a) relates to the usual situation of casting in a mould (i.e. without water cooling). Because of the

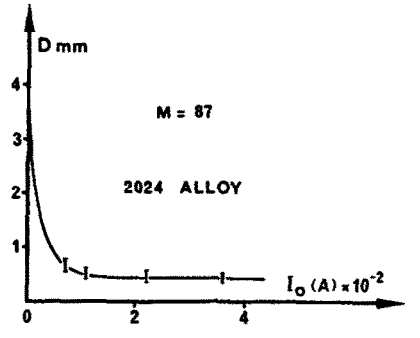

FIG. 17. Evolution of the mean equiaxed grain size with the electric current intensity (2024 alloy).

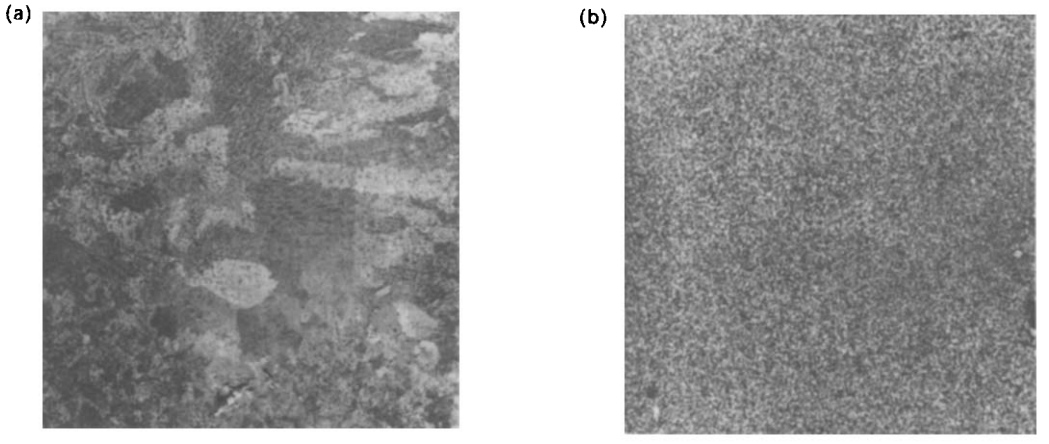

FIG. 18. Macrostructures of a 2024 aluminium alloy solidified without water cooling, in natural convection (a), and in the presence of crossed electric and magnetic fields (b), $M = 87$, $I_0 = 250$ A; size of the samples: 67×67 mm.

low heat extraction rate, the solidification takes place here without a preferential direction and a coarse equiaxed structure occurs. The specimen exhibited in Fig. 18(b) has been solidified in the presence of crossed electric and magnetic fields. It appears that a tremendous grain refinement is achieved, with regard to the sample presented in Fig. 18(a). Attention must be drawn to the fact that the mechanism of crystallization is here basically different from that characterizing the outward directional freezing in the presence of water cooling (Figs. 6 and 16). In the absence of water cooling, the floating nuclei which arise below the liquidus temperature are continuously segregated, as their formation proceeds, by the action of the centrifugal forces and accumulated in the vicinity of the outer wall (Figs. 10 and 12(b)). Under these circumstances, it appears that the direction of this inward solidification is inversed with respect to the case where the mould is water cooled. Moreover, it has been shown that the growing crystals are unmoved, when the solid fraction passes beyond 13% (Figs. 10 and 12(b)). Therefore, on account of the small amount of

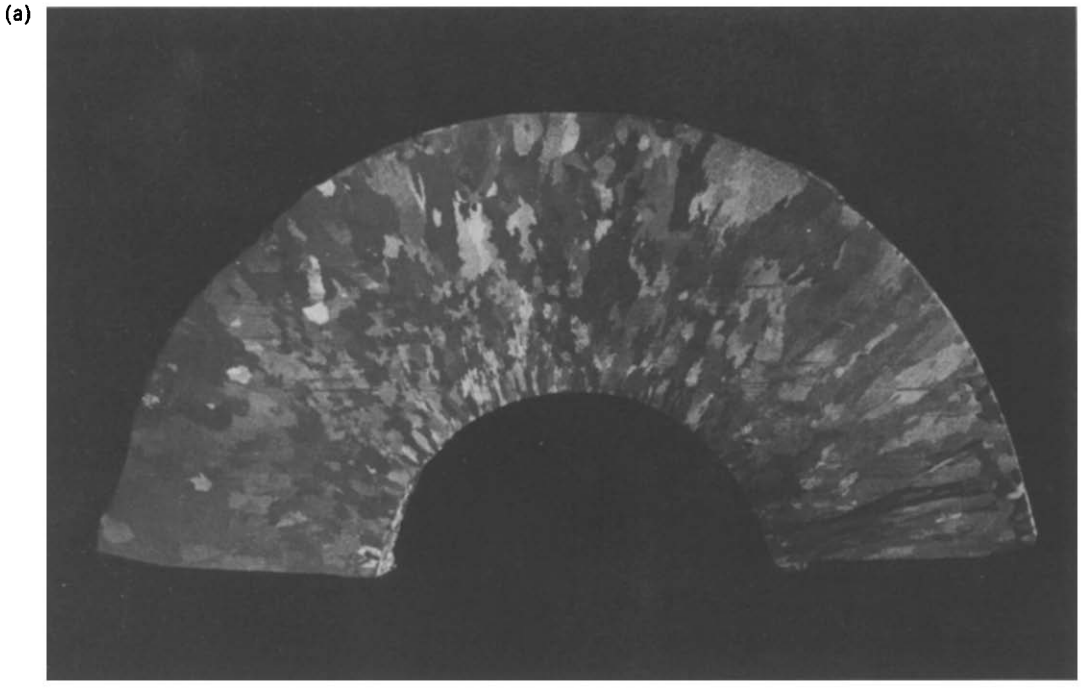

FIG. 19. Macrostructures of a 1050 aluminium alloy solidified in natural convection, (a) $\Delta T = 35$°C, in the presence of crossed electric and magnetic fields (b) $\Delta T = 35$°C, $M = 87$, $I_0 = 360$ A, and in the exclusive presence of a stationary magnetic field (c) $M = 87$, $I_0 = 0$; flow rate of cooling water: 1000 dm^3 h^{-1}; diameter of the samples: 170 mm.

(b)

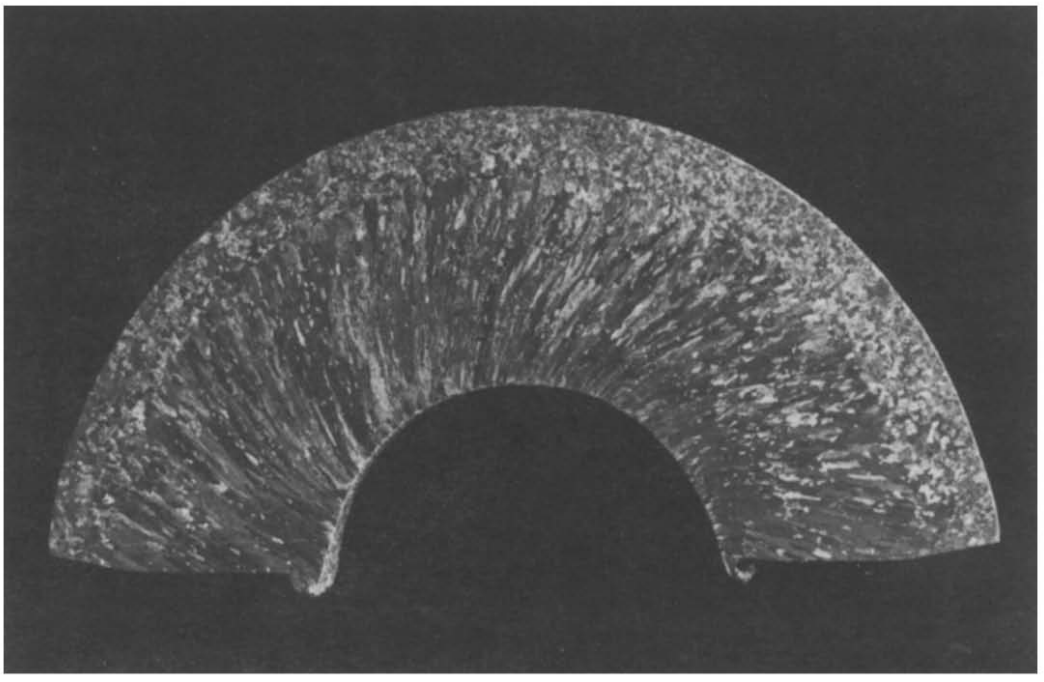

(c)

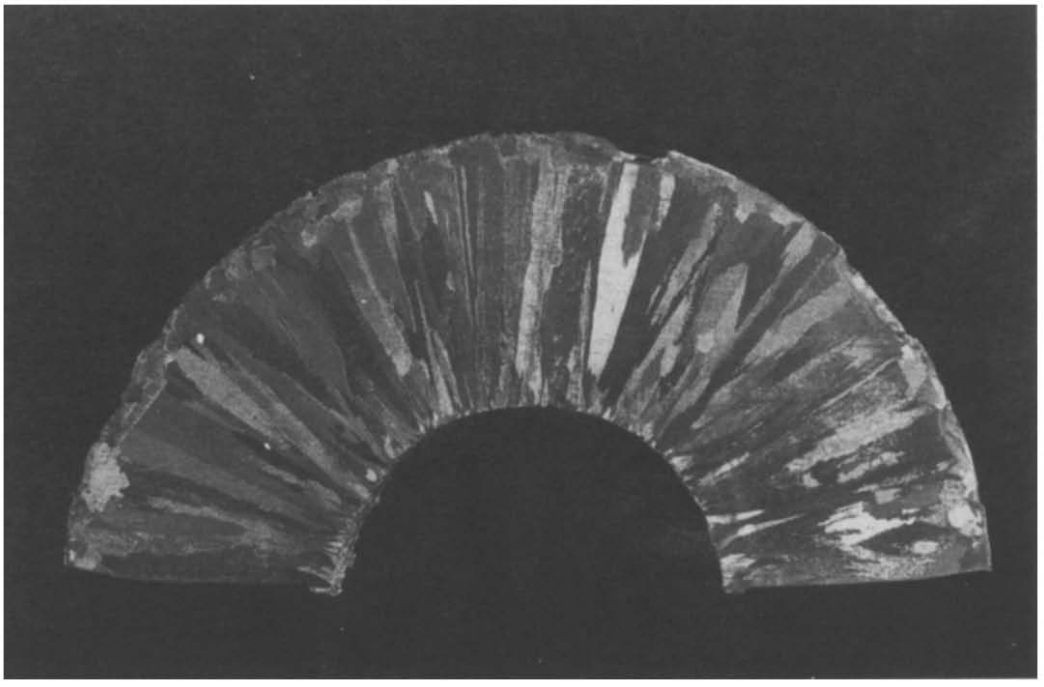

FIG. 19.—*Continued.*

liquid phase which surrounds these small equiaxed crystals, their growth is necessarily restricted. As an example, it is easy to show that a crystal of an ultimate grain size of 200 μm (i.e. at the freezing completion), originates from the growing of an unmoved segregated crystal of about 100 μm. Accordingly, inside our experimental range, the maximum size of the moving crystal, suspended in the mixture, cannot be higher than 100 μm.

Another set of solidification experiments was performed from 1050 aluminium alloy and in the presence of water cooling. Complementary tests consisting of the examination of vertical slices, obtained in natural convection, showed that the crystallization was exclusively columnar. On account of a unicellular liquid metal flow, with fluid descending along the interface and rising along the hot wall, the columnar zone is sloped in the upstream direction to the inter-

face [17, 29]. The sample presented in Fig. 19(a), corresponds to a horizontal slice of 170 mm o.d., cut at the mid-height of the ingot, and shows the sections of the oblique columns.

The macrostructure exhibited in Fig. 19(b) has been obtained in the presence of an electromagnetically rotating flow. Its inspection shows that, under our experimental conditions (i.e. degree of stirring intensity and rate of heat extraction), it was impossible to achieve a fine grained equiaxed structure. This macrography reveals the presence of fine blade-shaped crystals, once again inclined against the stream [17, 29], while a coarse equiaxed structure, exclusively located within a peripheral area of about 12 mm thick, can be seen. Complementary thermal measurements established that the appearance of this latter region was connected with the total evacuation of the initial superheat inside the solidifying remaining melt. Finally, Fig. 19(c) displays a sample corresponding to the suppression of the rotating flow, obtained in the exclusive presence of the magnetic field B_0 (the electric current I_0 was previously cut off). In such a circumstance, it is well known that the fluid motion caused by the natural convection is considerably damped [16] and it results from this that the columnar crystal grows horizontally and radially. Furthermore, the comparison between Figs. 19(b) and (c) shows that the average column diameter is markedly reduced by the rotating stirring.

Hence, it appears that, from the solidification standpoint, the behaviour of such an alloy, characterized by a narrow freezing range, is very different from that of the 2024 alloy and quite similar to that already described in the case of a pure metal [17].

7. CONCLUSIONS

The influence of rotating aluminium alloy flows, driven by a stationary electromagnetic field, during freezing in a toroidal mould, was examined. The experiments were performed in the absence, and in the presence, of forced cooling. The investigated material was mainly an aeronautic aluminium alloy (2024), characterized by a wide crystallization range. A discussion was presented relating the crystal growth phenomena to the heat and fluid flow measurements. In the case of the solidification without forced cooling, the important role of the centrifugal acceleration on the evolution during freezing of the velocity, temperature and solid fraction distributions in the two-phase mixture has been revealed. In contrast to the case of the solidification in the presence of water cooling, it appears that the electromagnetic stirring results in the presence of radial temperature gradients; moreover, the freezing direction is reversed, on account of the migration of suspended equiaxed crystals toward the outer wall of the mould. The main metallurgical consequence is that, in each case, the rotation of the solidifying melt results in an extensive grain refinement and, hence, eliminates the need for a nucleating agent.

Moreover, subsidiary experiments concerning a 1050 aluminium alloy, characterized by a narrow interval of solidification, showed that, from the crystallographical viewpoint, the behaviour of such a material was similar to that of a pure metal.

Furthermore, the evolution of the electrical conductivity of the melt with the temperature (or with the solid fraction of the two-phase medium), was represented by an empirical relationship, obtained through a simple experimental technique using an annular mould.

Finally, it should be mentioned that, in this investigation, the electromagnetic stirring was not very intense (maximum velocity of the order of 0.5 m s^{-1}). However, a solidifying alloy possesses thixotropic properties, when it is very vigourously stirred, while in the freezing range [7]. This mixture, where the solid phase has the structure of fine rounded and non-dendritic particles suspended in a liquid matrix, is likely to move for high solid fractions, which can reach 0.6. A study of the rheological behaviour of these non-Newtonian slurries, as well as of the metallurgical and mechanical characteristics of the solidified two-phase medium, is currently in progress in our laboratory.

Acknowledgement—The solid fraction–temperature relationship, presented in Fig. 8 and related to the 2024 aluminium alloy, was provided by the Research Centre of the Aluminium Pechiney Society of Voreppe, France.

REFERENCES

1. J. Szekely and P. S. Chhabra, The effect of natural convection on the shape and movement of the melt–solid interface in the controlled solidification of lead, *Metall. Trans.* **1**, 1195–1203 (1970).
2. J. Szekely, *Fluid Flow Phenomena in Metal Processing*, pp. 204–228. Academic Press, London (1979).
3. A. W. Hills, S. L. Malhotra and M. R. Moore, The solidification of pure metals (and eutectics) under unidirectional heat flow conditions: II. Solidification in the presence of superheat, *Metall. Trans.* **B6**, 131–142 (1975).
4. C. Gau and R. Viskanta, Melting solidification of a metal system in a rectangular cavity, *Int. J. Heat Mass Transfer* **27**, 113–123 (1984).
5. C. Gau and R. Viskanta, Effect of natural convection on solidification from above and melting from below of a pure metal, *Int. J. Heat Mass Transfer* **28**, 573–587 (1985).
6. B. Webb and R. Viskanta, An experimental and analytic study of solidification in a binary mixture, *Proc. 8th Int. Heat Transfer Conf.*, Vol. 4, pp. 1739–1744. Hemisphere, New York (1986).
7. D. B. Spencer, R. Mehrabian and M. C. Flemings, Rheological behavior of Sn-15 Pct Pb in the crystallization range, *Metall. Trans.* **3**, 1925–1932 (1972).
8. H. S. Marr, Electromagnetic stirring: stepping stone to improved continuously cast products, *Iron Steel Int.* **2**, 29–41 (1979).
9. D. B. Spalding and N. H. Afgan, *Heat and Mass Transfer in Metallurgical Systems*. McGraw-Hill, New York (1981).

10. G. Abbaschian and S. David, Grain refinement in castings and welds, *Metall. Soc. A.I.M.E.* 3–63 (1983).
11. A. A. Tsavaras and H. D. Brody, Electromagnetic stirring and continuous casting—achievements, problems and goals. *J. Met.* **1**, 31–37 (1984).
12. Ch. Vivès and B. Forest, CREM : a new casting process, Part I : fundamental aspect, light metals, *Metall. Soc. A.I.M.E.* 769–778 (1987).
13. K. H. Spitzer, M. Dubke and K. Schewerdtfeger, Rotational electromagnetic stirring in continuous casting or round strands, *Metall. Trans.* **B17**, 119–131 (1986).
14. H. Kodoma, E. Nyama, M. Horiguchi, Y. Numata, T. Kimura et M. Endo, La solidification de billettes dans la lingotière d'une coulée continue de type rotatif synchronisé, *Revue Métall., C.I.T.* **6**, 521–533 (1983).
15. Ch. Vivès and Ch. Perry, Effects of electromagnetic stirring during the controlled solidification of tin, *Int. J. Heat Mass Transfer* **29**, 21–33 (1986).
16. Ch. Vivès and Ch. Perry, Effects of magnetically damped convection during the controlled solidification of metals and alloys, *Int. J. Heat Mass Transfer* **30**, 479–496 (1987).
17. Ch. Vivès, Effects of a forced Couette flow during the controlled solidification of a pure metal, *Int. J. Heat Mass Transfer* **31**, 2047–2062 (1988).
18. L. Labarre, R. James, J. Witters, R. O'Malley and M. Emptage, Difficulties in grain refining aluminium lithium alloys using commercial Al–Ti and Al–Ti–Bor master alloys, *J. Phys.* Supplément au No. 9, **48**, 93–102 (1987).
19. M. Birch and A. Cowell, Titanium carbon aluminium : a novel grain refiner for aluminium lithium alloys, *J. Phys.* Supplément au No. 9, **48**, 103–108 (1987).
20. O. Ilegbusi and J. Szekely, On the flow criteria for suspending solid particles in inductively stirred melts : Part I : Newtonian behavior, *Metall. Trans.* **B19**, 557–562 (1988).
21. P. Rohatgi, S. Das and T. Dan, Cast aluminium–graphite composites—a potential engineering material, *J. Instn Engrs India Metall. Mater. Sci. Div.* **67**, 77–83 (1987).
22. R. Ricou and Ch. Vivès, Local velocity and mass transfer measurements in molten metals using an incorporated magnet probe, *Int. J. Heat Mass Transfer* **25**, 1579–1588 (1982).
23. H. C. Lee, J. W. Evans and Ch. Vivès, Velocity measurement in Wood's metal using an incorporated magnet probe, *Metall. Trans.* **B4**, 734–736 (1984).
24. J. A. Shercliff, *A Textbook of Magnetohydrodynamics*. Pergamon Press, Oxford (1965).
25. G. I. Taylor, Stability of a viscous liquid contained between rotating cylinders, *Phil. Trans. R. Soc. London* **A223**, 289–343 (1923).
26. G. Cognet, Les étapes vers la turbulence dans l'écoulement de Couette–Taylor entre cylindres co-axiaux, *J. Méc. Theorique Appliquée* numéro spécial, 7–44 (1984).
27. A. Chambarel, R. Ricou and Ch. Vivès, Les méthodes de diagnostics en magnétodynamique des métaux fondus, *J. Méc. Appliquée* **5**, 453–482 (1981).
28. Ch. Vivès and R. Ricou, Electromagnetic study of continuous electromagnetic casting of aluminium alloys, *Metall. Trans.* **B16**, 377–384 (1985).
29. B. Chalmers, *Principle of Solidification*. pp. 270–276. Krieger, Malabar, Florida (1982).
30. T. Takahashi, K. Ichikawa, M. Kudou and K. Shimahara, The effect of fluid flow on the macrosegregation in steel ingot, *Trans. I.S.I.J., Japan* **16**, 283–291 (1976).

EFFETS HYDRODYNAMIQUE, THERMIQUE ET CRYSTALLOGRAPHIQUE D'UN ECOULEMENT TOURNANT ENTRAINE ELECTROMAGNETIQUEMENT DURANT LA SOLIDIFICATION D'ALLIAGES D'ALUMINIUM

Résumé—On étudie l'influence d'écoulements rotatifs d'alliages d'aluminium, entraînés par un champ électromagnétique stationnaire, pendant leurs solidifications dans un moule toroïdal. Les expériences sont réalisées en absence, et en présence, d'un refroidissement forcé. Le rôle important de l'accélération centrifuge sur l'évolution, pendant la solidification, des distributions de vitesse, température et fraction solide dans le milieu diphasique, est mis en évidence. Dans le cas d'un alliage caractérisé par un large intervalle de solidification, la rotation du bain métallique se traduit par un affinage de la structure équiaxe. De plus, une technique expérimentale permettant la détermination de la conductivité électrique du bain au dessus de la température du liquidus, ainsi qu'à l'intérieur de l'intervalle de solidification, est proposée.

DIE HYDRODYNAMISCHEN, THERMISCHEN UND KRISTALLOGRAFISCHEN WIRKUNGEN EINER ELEKTROMAGNETISCH GETRIEBENEN ROTATIONSSTRÖMUNG IN VERFESTIGENDEN SCHMELZEN AUS ALUMINIUMLEGIERUNG

Zusammenfassung—Die Verfestigung einer durch ein stationäres elektromagnetisches Feld angetriebenen Rotationsströmung einer Aluminiumlegierung in einer Torusform wird untersucht. Die Versuche werden mit und ohne Kühlung ausgeführt. Es zeigt sich der wichtige Einfluß der Zentrifugalbeschleunigung auf die Verteilung von Geschwindigkeit, Temperatur und Festkörperanteil im Zweiphasengemisch bei der Verfestigung. Bei Legierungen mit einem breiten Kristallisationsbereich führt die Rotation der verfestigenden Schmelze zu einer ausgeprägten äquiaxialen Gefügeverfeinerung. Ein Verfahren zur experimentellen Bestimmung der elektrischen Leitfähigkeit der Schmelze oberhalb der Verflüssigungstemperatur und im Erstarrungsbereich wird vorgeschlagen.

ГИДРОДИНАМИЧЕСКИЙ, ТЕПЛОВОЙ И КРИСТАЛЛОГРАФИЧЕСКИЙ ЭФФЕКТЫ ТЕЧЕНИЯ, ВРАЩАЮЩЕГОСЯ ПОД ДЕЙСТВИЕМ ЭЛЕКТРОМАГНИТНОГО ПОЛЯ В ЗАТВЕРДЕВАЮЩИХ АЛЮМИНИЕВЫХ СПЛАВАХ

Аннотация—Исследуется эффект вращения течений алюминиевых сплавов под действием стационарного электромагнитного поля в процессе замораживания в тороидальной прессформе. Эксперименты проводятся как при отсутствии, так и при наличии вынужденного охлаждения. Установлено сильное влияние центробежного ускорения на развитие профилей скорости, температуры и твердой фракции в процессе замораживания. В случае сплава, характеризуемого широким диапазоном кристаллизации, вращение затвердевающего расплава приводит к существенному улучшению равноосной структуры. Предложена экспериментальная методика, позводяющая определить электроводность расплава при температуре выше ликвидуса, а также в диапазоне замораживания.